Journal of Molecular Structure 1224 (2020) 129065

Contents lists available at ScienceDirect

Journal of Molecular Structure

journal homepage: www.elsevier.com/locate/molstr

Growth, spectral, laser damage and hirshfeld surface studies on configurationally locked 2-(3-(4-hydroxystyryl)-5,5-dimethylcyclohex-2-enylidene) malononitrile (OH1) single crystal- A potential terahertz emitter

S. Karthick[a,b], A. Santha[a], D. Ganesh[c], K. Thirupugalmani[d], S. Ganesamoorthy[e], A.K. Chaudhary[c], S. Brahadeeswaran[a,*]

[a] Crystal Research Laboratory, Department of Physics, Bharathidasan Institute of Technology, Anna University, Tiruchirappalli-620024, India
[b] Department of Physics, Muthayammal Engineering College, Rasipuram, Namakkal-637 408, India
[c] Advanced Center of Research in High Energy Materials (ACRHEM), University of Hyderabad, Hyderabad-500046, India
[d] Department of Physics, ERK Arts and Science College, Dharmapuri 636905, India
[e] X-ray Scattering and Crystal Growth Section, Materials Science Group, CMPD, IGCAR, Kalpakkam, India

ARTICLE INFO

Article history:
Received 26 June 2020
Revised 9 August 2020
Accepted 10 August 2020

Keywords:
OH1 single crystals
Laser damage threshold
Hirshfeld surface studies
Nonlinear optics
Terahertz generation

ABSTRACT

We report on the growth, spectral, optical, laser damage and Terahertz (THz) wave generation studies and Hirshfeld analysis of the pyrrolidine-based, configurationally locked, polyene single crystals 2-(3-(4-hydroxystyryl)-5,5-dimethylcyclohex-2-enylidene) malononitrile (OH1), a potential organic material for THz generation. The laboratory synthesized OH1 was verified for its composition and crystalline phase using Carbon–Hydrogen–Nitrogen (CHN) analysis and powder X-ray diffraction method respectively. The functional groups of OH1 were confirmed through Fourier transformed infrared analysis whereas its band gap energy was calculated using the UV–Vis spectrum recorded on (100) plate of thickness of about 1 mm. The laser damage studies performed by employing Q-switched Nd:YAG laser revealed that the OH1 crystals could withstand laser fluences of the order of about 2.21 GW/ cm^2.Further, the OH1 single crystals were effectively used for the generation of intense THz waves using indigenously developed setup which comprises of a Ti: Sapphire laser (with 140 fs pulses) and detection using a pyroelectric sensor. Furthermore, 3D Hirshfeld surfaces and 2D finger print plots of OH1 were supportive in decoding the intermolecular interaction behaviour and the packing structure of the crystals.

1. Introduction

In recent years there has been progressive growth in the field of generation and detection of Terahertz (THz) waves as they possess interesting features such as low energy, non-ionizing and non-invasive [1–7] which make them suitable for applications in the areas of homeland security, biological imaging, non-destructive evaluation, etc. [8–10]. Nonlinear optical (NLO) methods such as optical rectification (OR) and difference frequency generation (DFG) are being routinely employed to generate the THz waves using potentially NLO active organic materials such as 4-N,N-dimethylamino-4′-N′-methylstilbazoliumtosylate (DAST) [11,12], N-benzyl-2-methyl-4-nitroaniline (BNA) [3], 4-dimethylamino-N-methyl-4-stilbazolium-p-chlorobenzenesulfonate (DASC) [13], N,N-dimethylamino-4′-N′-methylstilbazolium 2,4,6-trimethylbenzenesulfonate (DSTMS) [14], 2-(3-(4-hydroxystyryl)−5,5-dimethylcyclohex-2-enylidene) malononitrile (OH1) [15], (2-(5-methyl-3-(4-(pyrrolidin-1-yl)styryl)cyclohex-2-enylidene) malononitrile) (MH2) [16] as they possess relatively low dielectric constant and large nonlinear optical susceptibilities as compared to those of inorganic materials [17–19]. However, device fabrication with such organic THz crystals is still hindered by problems such as difficulties in growing reproducibly large size crystals, stability in normal ambient, incorporation of foreign particles and/or solvent inclusions in the crystals and less robust against strong optical pumping etc. and are required to be optimized [20,21]. amongst the crystals mentioned above, the OH1, a configurationally locked, organic phenolic polyene and non-ionic organic compound, whose crystal

* Corresponding author. Department of Physics, University College of Engineering (UCE), Bharathidasan Institute of Technology (BIT) Campus, Anna University, Tiruchirappalli-620024, Tamil Nadu, India.
E-mail address: sbrag67@yahoo.com (S. Brahadeeswaran).

https://doi.org/10.1016/j.molstruc.2020.129065
0022-2860/

structure was reported by T. Kolev et al.in the year 2001 [22], was identified as a potential THz emitter (almost a decade later) due to its excellent NLO properties [23–25]. Further, the OH1 cannot be dissolved in water and hence its hydrated form [26], which could hinder its THz generation efficiency, is naturally avoided. In the present manuscript we report our results on synthesis, compositional analysis, transmission properties, laser damage resistance, THz generation and Hirshfeld Surface studies of OH1. It is presented that the laser damage resistance of this material is comparable to other organic NLO and THz materials and that the OH1 molecules interact with each other predominantly through H···H interactions followed by H···N/N···H interactions.

2. Experimental procedure

2.1. Materials synthesis, microanalysis and growth of OH1

The OH1 was synthesized by means of Knoevenagel condensation of reacting isophorone (0.66 g, Sigma) and malononitrile (1.328 g, Sigma) using N, N, dimethylformamide as a solvent and piperidine acetate as a catalyst at room temperature. Subsequently, the obtained 3,5,5-trimethyl(cyclohex-2-enylidene) malononitrile precipitate was recrystallized using ethanol and reacted with equimolar ratio of 4-hydroxybenzaldehyde where chloroform was used as a solvent and piperidine acetate as a catalyst. The synthesis procedure and reaction scheme of OH1 is shown in Scheme. 1. The final product which appeared orange-red in colour was recrystallized several times using chloroform and purified by column chromatography on silica gel. The Carbon–Hydrogen–Nitrogen (CHN) test was performed for the purified OH1 powder sample using CHN (Vario EL III) elemental analyser. The results of microanalysis of the purifiedOH1 compound revealed that, there was a good agreement with the theoretically computed values (Table 1). The OH1 single crystals were grown by methanol, which has been already reported as a suitable solvent, by employing isothermal solvent evaporation solution growth technique. By this method, single crystals of OH1 (shown in Fig. 1) with typical dimensions of 5 × 3 × 1 mm^3 were harvested in about 24 days duration. From the figure it could be seen that the OH1 crystals were platy in nature and that the growth takes place predominantly along [100] direction; this is due to the fact that the OH1 molecule is nearly planar with an exception of $C(CH_3)_2$ group [22]. Further, it has already been shown by us that the rate at which the desolvation of solute molecules takes place near the growing crystal-solution interface plays crucial role in deciding the development of crystal planes [3]. These aspects facilitate the growth of OH1 crystals with well-developed and smooth {100} planes and the as-grown crystals could be directly used (thereby avoiding the tedious post-processing (such as polishing)) for the generation of THz waves [27].

Table 1
Microanalysis of OH1 molecule ($C_{19}H_{18}N_2O$).

Elements	Calculated (%)	Experimental (%)
Carbon	78.59	78.62
Hydrogen	6.25	6.22
Nitrogen	9.65	9.69
Oxygen	5.51	

3. Results and discussion

3.1. X-ray diffraction (XRD) analysis

The as grown OH1 single crystal was used to analyse the lattice constants by Enraf- Nonius CAD-4/MACH 3 Diffractometer, with Mo Kα radiation (k = 0.71073 Å). It was confirmed that, OH1 molecules crystallized with orthorhombic space group $Pna2_1$andwas in good agreement with the reported values (Table 2). Subsequently, the polycrystalline powder pulverized from selected small single crystals was subjected to powder X-ray diffraction analysis using XPERT-PRO powder X-ray diffractometer (Cu-Kα radiation, 40 kV, 30 mA) to confirm the phase formation of OH1.Further, crystallographic Information File (CIF) data of OH1,

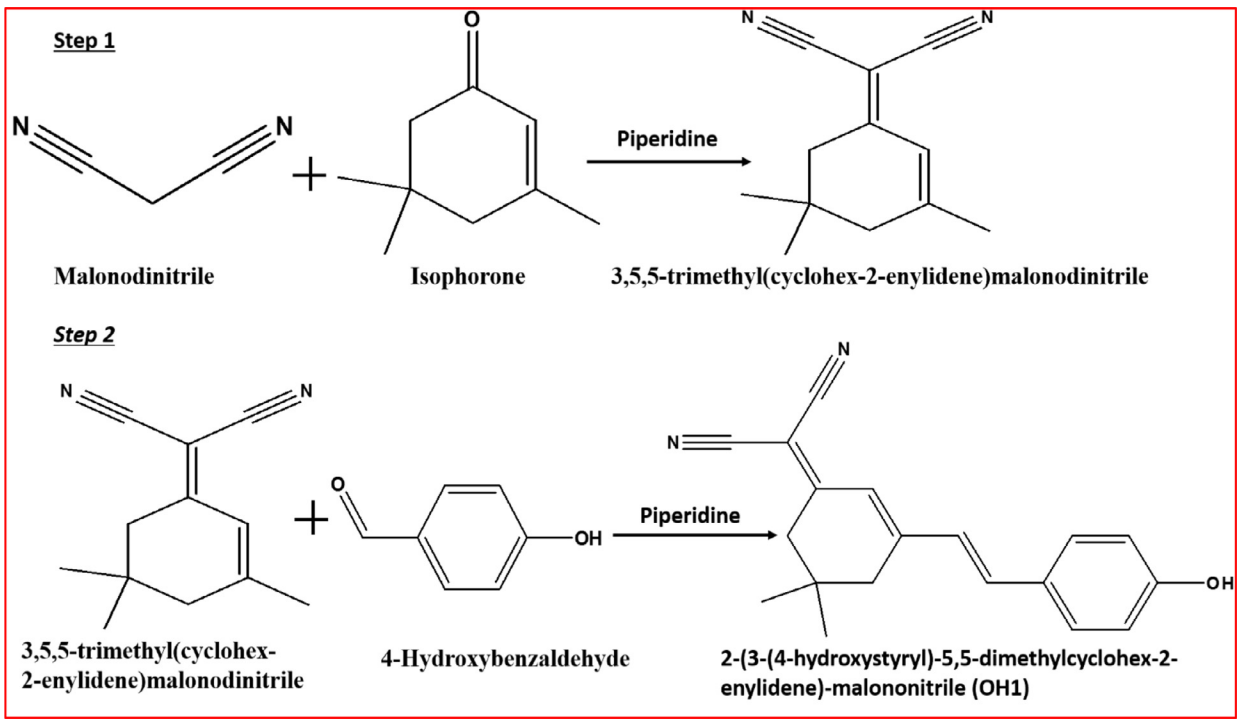

Scheme 1. Synthesis and reaction scheme of OH1.

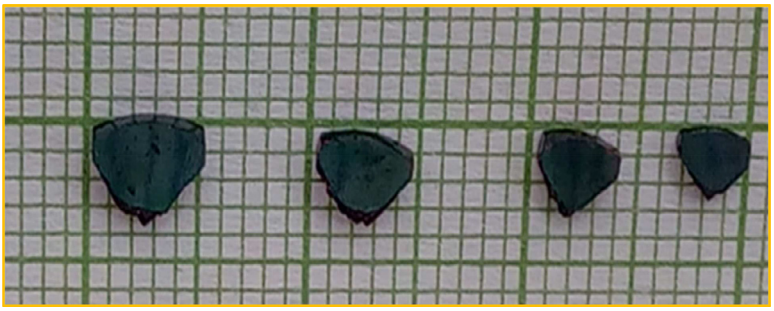

Fig. 1. Photograph of as grown OH1 single crystals.

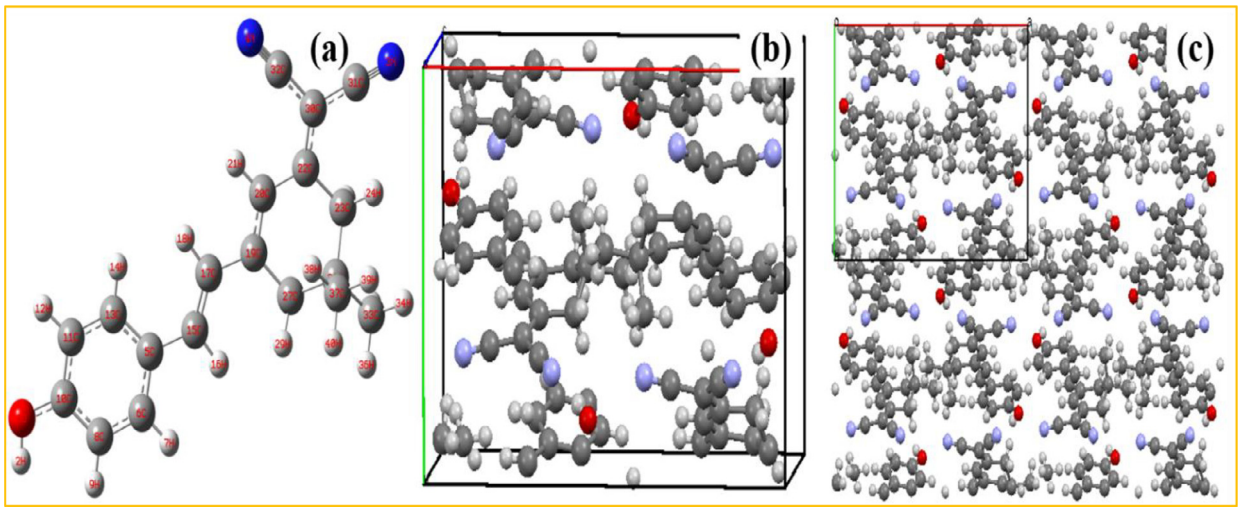

Fig. 2. (a) Optimized molecular structure (c) The molecular packing in a unit cell and (d) its extended network of OH1 molecule.

Table 2
Lattice parameter values of OH1 single crystal.

Parameters	Present work	Reported [22]
a(Å)	15.440	15.4413 (3)
b(Å)	10.994	10.9988 (3)
c(Å)	9.568	9.5699 (2)
α	90°	90°
β	90°	90°
γ	90°	90°
Volume (Å3)	1624.14	1625.31 (6)

obtained from Cambridge Crystallographic Data Centre (CCDC)and MERCURY program, [28]was used to plot the simulated XRD pattern and various planes were also indexed and compared with experimental one (Fig. 4).From the figure it could be seen that both the XRD data agreed well with each other. Moreover, the BFDH morphology of OH1 single crystal was elucidated and is shown in Fig. 3. From the figure it could be understood that the {100} planes were the prominent crystallographic planes and there was a good agreement with the experimentally observed results. The molecular structure along with the numbering scheme of atoms is shown in Fig. 2a whereas the molecular packing in a unit cell of OH1 and its extended network were shown in Fig. 2b and c respectively.

3.2. FTIR spectra of OH1

FTIR spectrum of OH1 was recorded by employing Fourier transformed infrared spectrometer (JASCO-FTIR 6300; wavelength range 400–4000 cm^{-1}) using the KBr pellet technique with a resolution of 4.0 cm^{-1}. The recorded FTIR spectrum of OH1 was shown

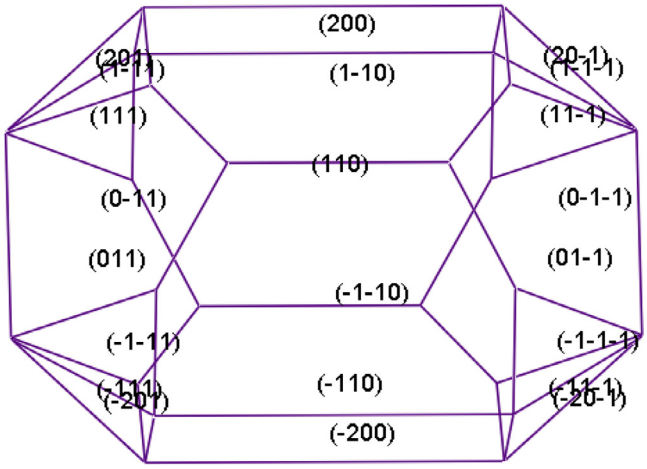

Fig. 3. BFDH morphology of OH1 single crystal.

in Fig. 5. The strong absorption peaks occurred at 3363 $cm^{-1}$and 2950 cm^{-1} could be attributed to the OH stretching vibrations. The very sharp band seen at2216 $cm^{-1}$was assigned to the stretching of C≡N in malononitrile. Following this, the peaks seen at 1602 and 1553 cm^{-1} in FTIR spectrum were due to the stretching of $C = C$ in aromatic ring. Similarly, the peak at 1367 and 1268 cm^{-1} could also be attributed to the C–H-stretching in aromatic ring whereas peaks at 958 and 842 cm^{-1} were assigned to the deformation of C–H out of plane bending. The IR band at 641 cm^{-1} was due to the stretching of C–H bond. The FTIR spectrum revealed that it contained nearly all the peaks expected for OH1.

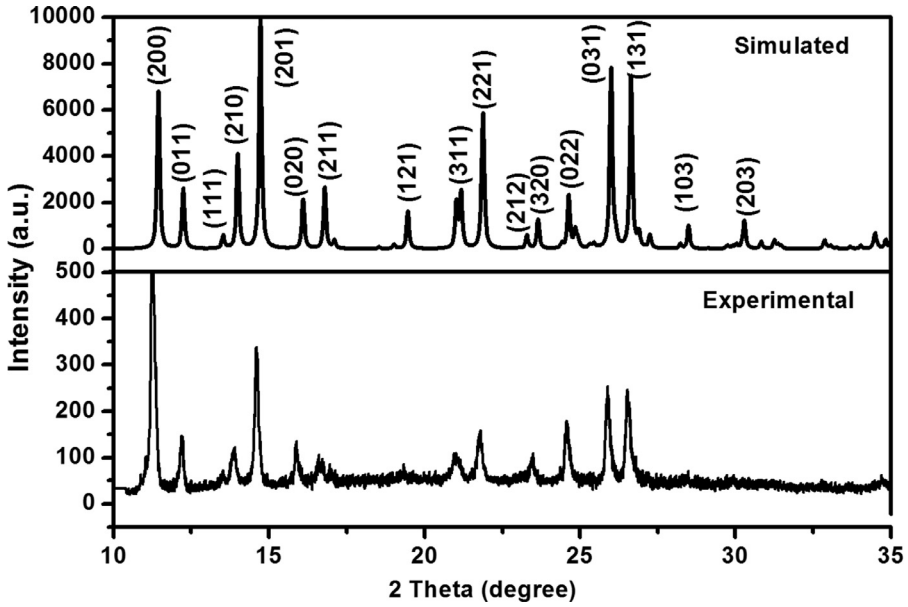

Fig. 4. Powder XRD pattern of OH1.

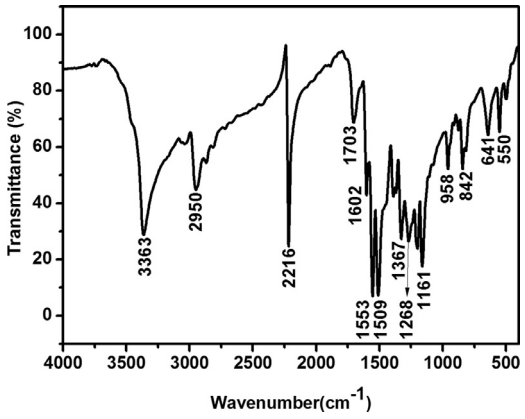

Fig. 5. FTIR Spectrum of OH1.

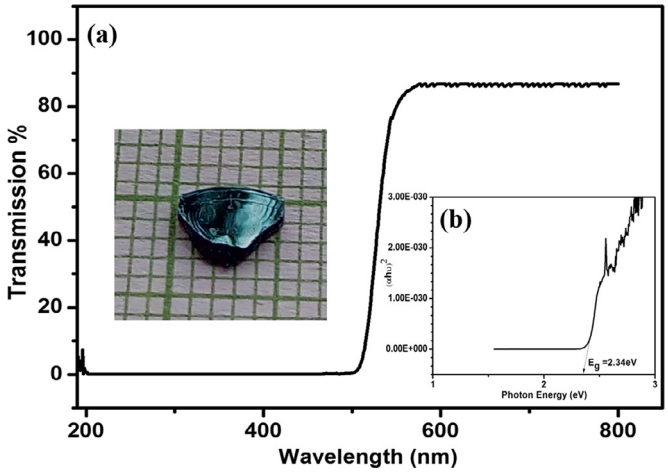

Fig. 6. **(a)**UV–Vis Transmittance spectrum of OH1 single crystal and (**b**) Band gap calculation using Tauc's plot.

3.3. Transmission spectrum

The transmission spectrum of polished OH1 single crystal ((100) plane) of thickness 0.92 mm was recorded using JASCO V-650 spectrophotometer at room temperature with a wavelength accuracy of ± 0.2 nm (shown in Fig. 6a). The transmission spectrum showed that OH1 single crystal possessed a good transparency and that the maximum transparency was around 86% in the wavelength range 560–800 nm. The lower cutoff wavelength of the OH1 single crystal was found to be about 504 nm and this could be attributed to the strong electronic transitions from the ground state to excited state. From the inset Fig. 6b., (tauc's plot [29]), it could be seen that the band gap energy (Eg) of OH1 crystal was found to be about 2.34 eV, which is slightly higher than the reported value [18].

3.4. Laser damage threshold measurements

Prior knowledge on the ability of the crystals to withstand higher optical power densities i.e. their laser damage threshold values is of crucial importance when they are used for THz wave applications and to ensure their photochemical stability [30]. Although it is a destructive method, the threshold values would pro-

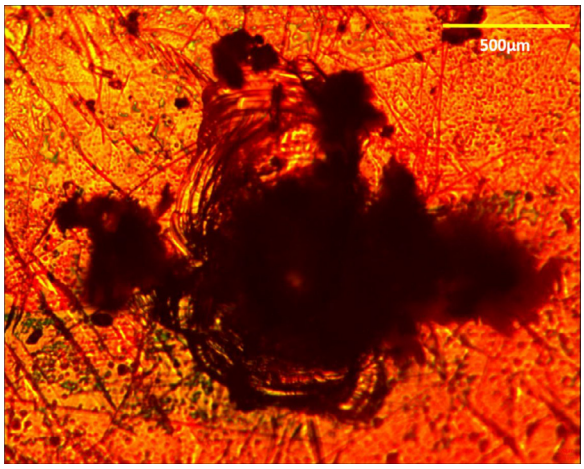

Fig. 7. Micrograph of laser damage threshold measurement.

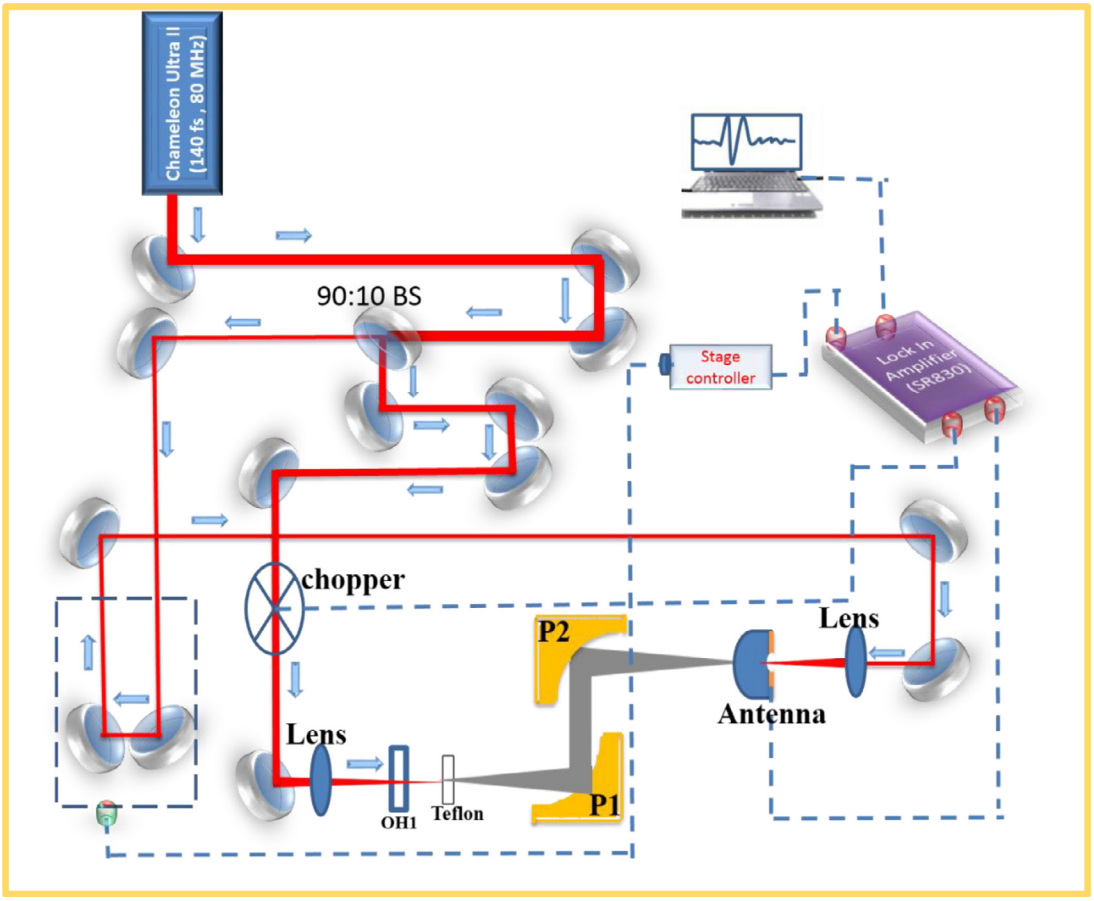

Fig. 8. Experimental schematic for THz generation and detection from OH1 crystal.

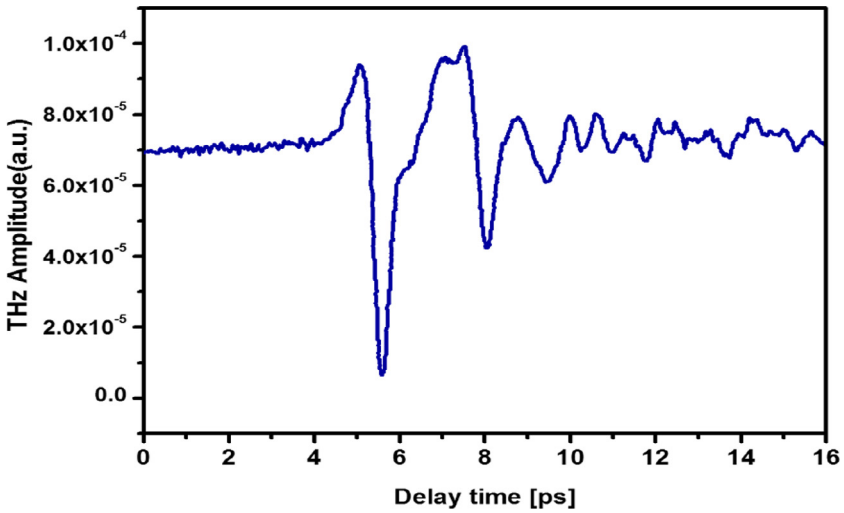

Fig. 9. Temporal profile of the electric field.

vide decisive upper limit for device fabrication. In the present investigation, the OH1 crystal was subjected to single shot laser damage threshold measurements using Q- switched Nd:YAG laser (wavelength 1064 nm; pulse width 10 ns and repetition rate 10 Hz). Initially, the as-grown OH1 single crystal was mounted on the goniometer in such a way that the laser radiation will impinge on (100) plane. The crystal was translated along X-Y plane of stage while increasing the incident power until the crystal got damaged. The power metre was used to record the energy density at which the crystal got damaged. The micrograph of the damaged location in OH1crystal is shown in Fig. 7. From the recorded micrograph of damage pattern, it could be seen that, the cracks were developed and the surface was uneven, which could be attributed to the melting and re-solidification of OH1. Further, it could be observed that, there were some greenish blobs around the damaged portion which also could be attributed to the re-solidification of OH1 species. The laser induced damage threshold value of OH1 was calculated using the formula $I = E/\tau\pi r^2$ [31] where I is the

Table 3
Comparison of laser damage threshold of few known organic NLO and THz crystals.

Organic NLO Crystals	Laser damage threshold value GW/cm^2	References
4-Dimethylamino-N-methyl-4-stilbazolium tosylate (DAST)	2.80	[32]
4-Dimethylaminopyridinium-3,5-dicarboxybenzoate trihydrate (DMAPB)	1.06	[33]
Guanidinium 4-nitrobenzoate (GuNB) and	2.55	[34]
Dimethyl amino pyridinium 4-nitrophenolate 4-nitrophenol (DMAPNP)	2.24	[35]
4-Bromo4-Nitrostilbene (BONS)	0.25	[36]
2-Amino pyridinium-4–hydroxy benzoate (2AP4HB)	2.13	[37]
2-Aminopyridine-4-nitrophenol-4-nitrophenolate (2AP4N)	2.12	[38]
2-Amino-6-methylpyridine-4-nitrophenol-4-nitrophenolate (2,6MAP4N)	1.34	[38]
2,6-Diaminopyridine-4-nitrophenol-4-nitrophenolate (2,6DAP4N)	2.94	[38]
2-(3-(4-Hydroxystyryl)−5,5-dimethylcyclohex-2-enylidene) malononitrile (OH1)	2.21	Present work

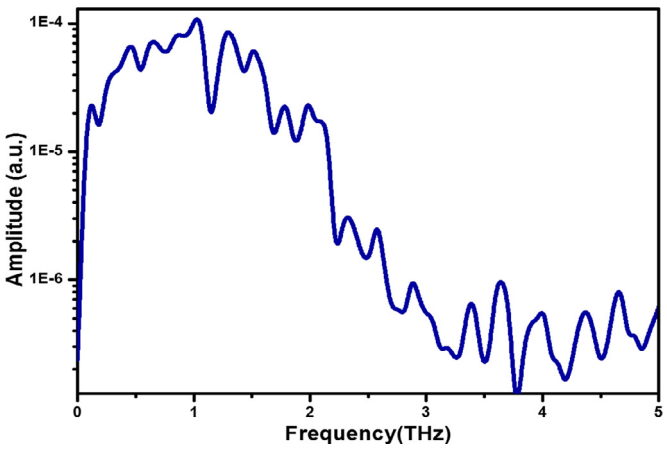

Fig. 10. Amplitude spectra of generated THz waves from OH1 single crystal.

energy in which the crystal gets damaged, E is input beam energy (mJ), ' τ ' is the pulse width (ns) and 'r' is the radius of the beam (mm).The evaluated single shot laser damage threshold power density of OH1 was about 2.21 GW/ cm^2. It is interesting to note that the laser damage value of OH1 was earlier reported to be 0.62 GW/ cm^2 for the same pulse width (10 ns) from the Nd:YAG laser [18]. However, it has not been stated in the earlier report whether the OH1 crystal was subjected to single shot or multiple shot laser fluences. In general, the single shot laser damage values will be higher than that for the multiple shot laser damage under identical experimental conditions. The laser damage threshold results of OH1 single crystal could be compared with other known organic NLO crystals (Table 3). From the table, it could be observed that the laser damage threshold of OH1 is comparable to other organic NLO and THz crystals listed [32–38].

3.5. THz generation

The THz generation efficiency of as-grown OH1 single crystal was studied by employing the experimental set up as shown in Fig. 8. The Ti: Sapphire femto-oscillator (Coherent Chameleon Ultra II) was used as a laser source which delivers laser pulses of ~140 fs and a repetition rate of 80 MHz. The output average power was attenuated by using Eskpla variable attenuator. The attenuated laser pulses with relatively lower power than the laser damage threshold (to prevent crystal from damage) was allowed to incident on (100) plane of the high quality as grown OH1 single crystal of thickness 0.72 mm. The crystal was housed in a Teflon holder that was kept in an optical rotator for the generation of THz waves. The pump and probe beam powers were ~ 200 mW, and ~170 mW for emission and detection of THz radiation, respectively. Teflon sheet was used to filter out the unconverted pump beam from the OH1crystal. The thus generated THz frequencies were detected by dipole photoconductive antennas (gap ~5 μm, length ~20 μm) using photoconductive sampling technique. The antenna output was connected to preamplifier which was fed to the Lock-in Amplifier (Model no.SR830). The S/N ratio was enhanced using mechanical chopper operating at 1.569 kHz frequency. The probe beam path length was varied to measure temporal profile of THz radiation. The terahertz temporal field and the results of THz generation obtained from OH1 crystals are shown in Figs. 9 and 10 respectively. From the Fig. 10 it could be seen that the OH1 single crystals are capable of generating THz waves in the range of 0.1 to 3 THz (in the lower range). It has already been reported by Jazbinsek et al. that the OH1 is the material with highest THz efficiency as compared to many organic crystals at low frequencies, especially below 3 THz [30]. This low frequency range, which is nearly similar to another non-ionic Terahertz crystal BNA as reported by us recently for the frequency range 0.1 to 2.0 THz [39], will be very useful in detecting biomolecules and explosives as they exhibit their

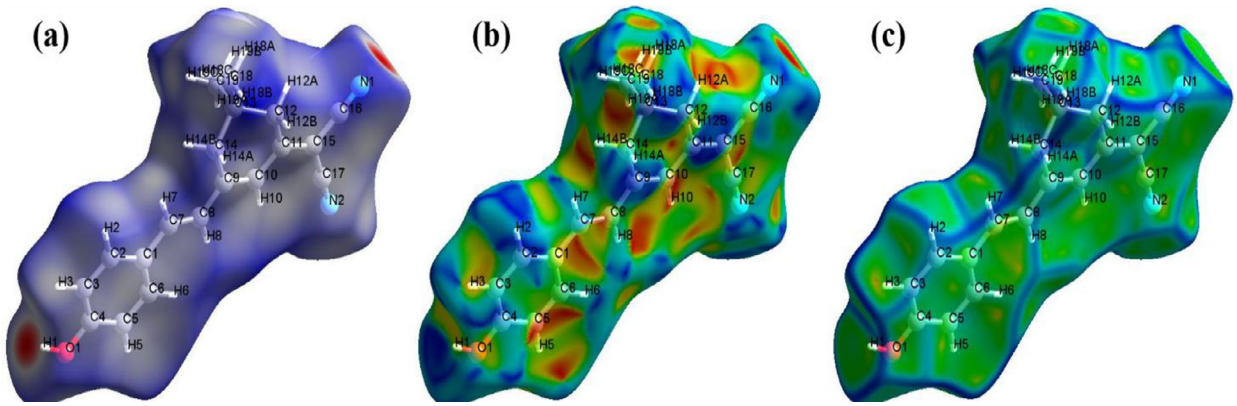

Fig. 11. 3D Hirshfeld surfaces mapped with (a) Normalized contact distance (d_{norm}) (b) Shape index (c) Curvedness of OH1 molecule.

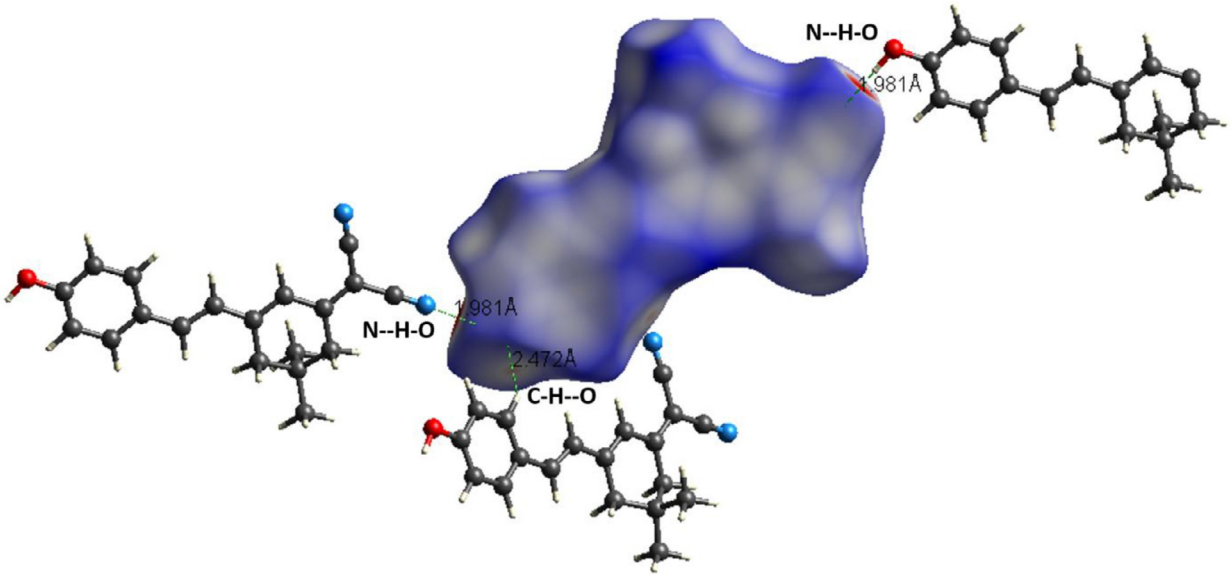

Fig. 12. Hirshfeld surface for OH1 molecule mapped with d *norm* and neighbouring molecules associated with close contacts are shown.

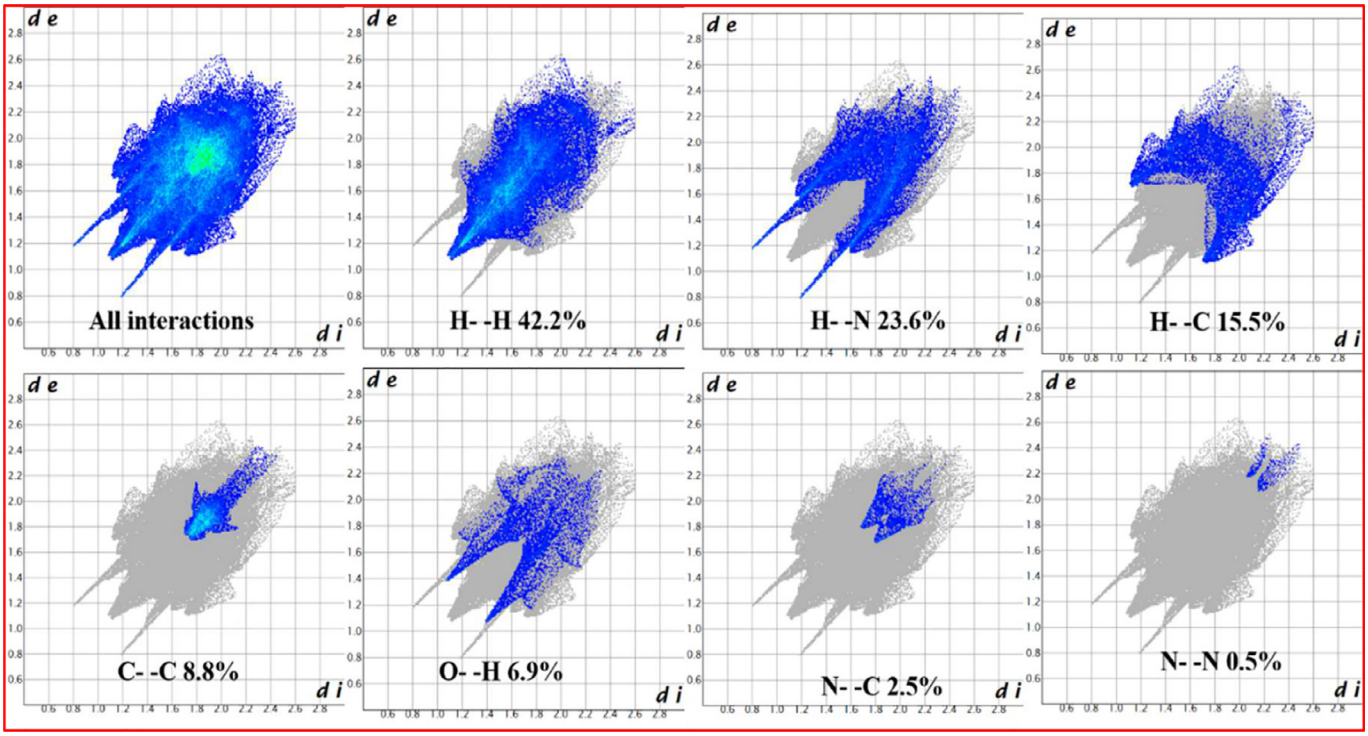

Fig. 13. 2D Finger print plots of various intermolecular interactions showing the percentages of contacts.

characteristic finger prints in this range [40,41] and many materials which are opaque in the visible range are transparent at these lower frequencies [42].The dips observed in the THz spectrum between 0.1 and 3 THz for the OH1 crystals explored could be attributed to the molecular phonon and lattice phonon modes and the latter could arise from intermolecular interactions in the crystal.

3.6. Hirshfeld surface analysis

In order to gain more insight into the extraction of molecular properties from X-Ray diffraction data, schemes such as Wigner-Seitz (WS), Bader's Quantum Theory of Atoms in Molecules (QTAM), Hirshfeld partitioning (H) and Hirshfeld's partitioning with a surface (HS) have been proposed [43–45]. amongst them, in as early as 1977, the scheme H [43] provided a concept of dividing the electron density of a molecule into continuous atomic fragments so that a molecular weight function w(r) could be defined by extracting overlapping, continuous molecular fragments from experimental electron densities in crystals as follows [44]:

$$w(r) = \sum_{A \in molecule} \rho_A(r) / \sum_{A \in crystal} \rho_A(r) = \rho_{promolecule}(r)/\rho_{procrystal}(r)$$

where $\rho_A(r)$ is a spherically averaged atomic electron density function centred on Nucleus A, and the promolecule and procrystal are formed by summing the overlapping constituent ground-state

(non-interacting) atoms. It is further suggested that the w(r) lies between 0 and 1 and that the integration over the product w(r)ρ(r), the weighted electron density, provides molecular properties. In this approach every constituent atom contributes to the molecular electron density depending upon its own charge density in a way much similar to partners in the stockholders' corporation [43]. Later, in 1997, the Hirshfeld partitioning with a surface (HS) scheme was suggested by Spackman by defining a molecular electron density in the weighted region of w(r) $\geq$ 0.5 (instead of weighting the electron density of crystal by w(r)) so that the contribution of promolecule exceeds that from all the neighbouring molecules. This approach provided convenient means of preventing the overlapping with the neighbouring molecules and still providing maximum proximity amongst them and thereby creating intermolecular voids [45]. For the present investigation, the three-dimensional (3D) Hirshfeld surface analysis and the two-dimensional (2D) intermolecular interactions of the OH1 molecule were carried out using Crystal Explorer 3.1 software package [46]. The mapping of normalized contact distance (d_{norm}), shape index and curvedness (shown in Fig. 11a, b & c respectively) have been performed by feeding its crystallographic data. From the figure it could be seen that the three characteristic colors such as red, blue and white appeared in the d_{norm} scheme belongs to the closer contacts with negative d_{norm} value, longer contacts with positive d_{norm} value and contacts equal to the Van der Waals separation ($d_{norm} = 0$) respectively. Further, d_e represents the distance from the Hirshfeld surface to the nearest nucleus external to the surface and d_i is nearest nucleus internal to the surface. The close contacts of the molecules are shown in Fig. 12 along with distances that combine both d_e and d_i, each normalised by the van der Walls radius. From the figure, the red–white–blue colouring scheme is used to distinguish it from the red–green–blue schemes, contacts shorter than van der Walls separations show up as red spots on a largely blue surface. The two shorter N- -H—O contacts of each distance 1.981 Å were characterized from two red spots, one at the left of the OH1 molecule and one at the right. The other contact is associated with C—H- -O of distance 2.472 Å. Fig. 13 shows the 2D Finger print plots of various intermolecular interactions showing the percentages of contacts. From the fingerprint histogram, it could be observed that the H••H bondings play predominant role in the intermolecular interactions with a contribution of 42.2% of the total Hirshfeld surface area whereas the H••N/N••H interactions, appeared as two distinct spikes in the 2D fingerprint plots, had 23.6% of the total Hirshfeld surface as a result of hydrogen bonding connections. The remaining contributions were from H••C (15.5%), C••C (8.8%) and other contacts. It is interesting to note that another non-ionic THz crystal BNA also exhibited similar behaviour for the H••H interactions (49.5%) [47] between the molecules followed, however, by nearly equal contributions (≈20%) from O••H and C••H bondings, unlike the H••N/N••H interactions in OH1 crystal.

4. Conclusions

In conclusion, the OH1 material was successfully synthesized in the laboratory and optical quality single crystals were grown from methanol solvent. The chemical composition of the purified OH1 was found to be identical with that of theoretically calculated values. The lattice parameters were analysed using single crystal X-ray diffraction analyses whereas the crystalline phase of the OH1wasconfirmed through powder X-ray diffraction analysis. The functional groups present in the OH1 compound were assigned through FTIR measurement. Further, higher transmission spectrum of about 85% was achieved from the polished OH1 single crystal owing to the purity of the staring material and optical quality of the grown crystal. Single shot laser damage threshold value was found to be 2.21 GW/ cm^2. The THz measurements made with this as grown OH1 single crystals revealed that, it could be a suitable candidate to realize their THz applications such as homeland security, communication, pharmaceutics, medicine and the detection of chemicals or explosives which exhibit fingerprints in between 0.1 to 3 THz range. The Hirshfeld surface analysis yielded the details regarding the 3D surfaces and 2D finger print patterns for a single molecule based on promolecule concept and the bonding contributions responsible for intermolecular interactions. Thus, by considering the above factors such as better optical transmission, large laser damage threshold value, efficient THz generation and surface analysis, it could be stated that OH1 single crystal could be a suitable candidate for THz generation and related applications.

Declaration of Competing Interest

None of the authors has any potential financial conflict of interest related to this manuscript.

CRediT authorship contribution statement

S. Karthick: Writing - original draft, Investigation, Conceptualization, Methodology, Software. **A. Santha:** Investigation, Formal analysis. **D. Ganesh:** Investigation, Formal analysis. **K. Thirupugalmani:** Investigation. **S. Ganesamoorthy:** Methodology, Funding acquisition. **A.K. Chaudhary:** Investigation, Funding acquisition. **S. Brahadeeswaran:** Writing - review & editing, Supervision, Project administration, Methodology, Funding acquisition.

Acknowledgements

The authors AS, SG and SB gratefully acknowledge the UGC-DAE Consortium for Scientific Research for their financial support through the grant CSR-KN/CRS-112/2018–19/1051 dated 26–12–2018. The authors AKC, DG gratefully acknowledge the financial support from the **DRDO**, Ministry of Defence, Govt. of India, ACRHEM (Phase –III).

References

[1] J.H. Jeong, B.J. Kang, J.S. Kim, M. Jazbinsek, S.H. Lee, S.C. Lee, I.H. Baek, H. Yun, J. Kim, Y.S. Lee, J.H. Lee, J.H. Kim, F. Rotermund, O.P. Kwon, High-power broadband organic THZ generator, Sci. Rep. 3 (2013) 1–8, doi:10.1038/srep03200.
[2] H. Adachi, T. Taniuchi, M. Yoshimura, S. Brahadeeswaran, T. Higo, M. Takagi, Y. Mori, T. Sasaki, H. Nakanishi, High-Quality Organic 4-Dimethylamino-N-methyl-4-stilbazolium Tosylate (DAST) Crystals for THz Wave Generation, Jpn. J. Appl. Phys. 43 (2004) 1121–1123, doi:10.1143/JJAP.43.L1121.
[3] K. Thirupugalmani, M. Venkatesh, S. Karthick, K.K. Maurya, N. Vijayan, A.K. Chaudhary, S. Brahadeeswaran, Influence of polar solvents on growth of potentially NLO active organic single crystals of *N*-benzyl-2-methyl-4-nitroaniline and their efficiency in terahertz generation, CrystEngComm 19 (2017) 2623–2631, doi:10.1039/C7CE00228A.
[4] H. Uchida, R. Yamazaki, K. Oota, K. Okimura, T. Minami, K. Takeya, K. Kawase, Organic Nonlinear Optical Single-Crystalline Thin Film Grown by Physical Vapor Deposition for Terahertz Generation, Cryst. Growth Des. 18 (2018) 4029–4036, doi:10.1021/acs.cgd.8b00388.
[5] M. Shalaby, C. Vicario, K. Thirupugalmani, S. Brahadeeswaran, C.P. Hauri, Intense THz source based on BNA organic crystal pumped at Ti:sapphire wavelength, Opt. Lett. 41 (2016) 1777–1780, doi:10.1364/OL.41.001777.
[6] J.Y. Choi, S.J. Lee, S.C. Lee, C.U. Jeong, M. Jazbinsek, H. Yun, B.J. Kang, F. Rotermund, O.P. Kwon, Quinolinium single crystals with a high optical nonlinearity and unusual out-of-plane polar axis, J. Mater. Chem. C 5 (2017) 12602–12609, doi:10.1039/C7TC04835A.
[7] I. McIntosh, B. Yang, S.M. Goldup, M. Watkinson, R.S. Donnan, Terahertz spectroscopy: a powerful new tool for the chemical sciences? Chem. Soc. Rev. 41 (2012) 2072–2082, doi:10.1039/C1CS15277G.
[8] K.S. Rao, A.K. Chaudhary, M. Venkatesh, K. Thirupugalmani, S. Brahadeeswaran, DAST crystal-based terahertz generation and recording of time resolved photoacoustic spectra of N_2O gas at 0.5 and 1.5 THz bands, Curr, Appl. Phys. 16 (2016) 777–783, doi:10.1016/j.cap.2016.04.009.
[9] B. Ferguson, X.C Zhang, Materials for terahertz science and technology, Nat. Mater. 1 (2002) 26–33, doi:10.1038/nmat708.
[10] M.C. Hoffmann, J.A. Fülöp, Intense ultrashort terahertz pulses: Generation and applications, J. Phys. D: Appl. Phys. 44 (2011) 1–17, doi:10.1088/0022-3727/44/8/083001.

[11] S. Brahadeeswaran, S. Onduka, M. Takagi, Y. Takahashi, H. Adachi, T. Kamimura, M. Yoshimura, Y. Mori, K. Yoshida, T. Sasaki, Twin-free and high quality DAST crystals-Effected through solutions of lower supersaturation coupled with isothermal solvent evaporation, Cryst. Growth Des. 6 (2006) 2463–2468, doi:10.1021/cg0505721.
[12] S. Brahadeeswaran, S. Onduka, M. Takagi, Y. Takahashi, H. Adachi, M. Yoshimura, Y. Mori, T. Sasaki, Growth of high-quality DAST crystals for THz applications, J. Cryst. Growth 292 (2006) 441–444, doi:10.1016/j.jcrysgro.2006.04.052.
[13] S. Brahadeeswaran, Y. Takahashi, M. Yoshimura, M. Tani, S. Okada, S. Nashima, Y. Mori, M. Hangyo, H. Ito, T. Sasaki, Growth of Ultrathin and Highly Efficient Organic Nonlinear Optical Crystal 4′-Dimethylamino-*N*-methyl-4-Stilbazolium *p*-Chlorobenzenesulfonate for Enhanced Terahertz Efficiency at Higher Frequencies, Cryst. Growth Des. 13 (2013) 415–421, doi:10.1021/cg300606g.
[14] Y. Li, J. Zhang, G. Zhang, L. Wu, P. Fu, Y. Wu, Growth and characterization of DSTMS crystals, J, Cryst. Growth 327 (2011) 127–132, doi:10.1016/j.jcrysgro.2011.05.005.
[15] O.P. Kwon, S.J. Kwon, M. Jazbinsek, F.D.J. Brunner, J.I. Seo, C. Hunziker, A. Schneider, H. Yun, Y.S. Lee, P. Gunter, Organic Phenolic Configurationally Locked Polyene Single Crystals for Electro-optic and Terahertz Wave Applications, Adv. Funct. Mater. 18 (2008) 3242–3250, doi:10.1002/adfm.20800633.
[16] J.Y. Seo, S.B. Choi, M. Jazbinsek, F. Rotermund, P. Gunter, O.P. Kwon, Large-Size Pyrrolidine-Based Polyene Single Crystals Suitable for Terahertz Wave Generation, Cryst. Growth Des. 9 (2009) 5003–5005, doi:10.1021/cg9009493.
[17] C.U. Jeong, B.J. Kang, S.H. Lee, S.C. Lee, W.T. Kim, M. Jazbinsek, W. Yoon, H. Yun, D. Kim, F. Rotermund, O.P. Kwon, Yellow-Colored Electro-Optic Crystals as Intense Terahertz Wave Sources, Adv. Funct. Mater. 28 (2018) 1801143 1-8, doi:10.1002/adfm.201801143.
[18] D. Bharath, S. Kalainathan, Dielectric, optical and mechanical studies of phenolic polyene OH1 organic electrooptic crystal, Optics & Laser Technology 63 (2014) 90–97, doi:10.1016/j.optlastec.2014.03.017.
[19] J. Kim, S.H. Lee, S.C. Lee, M. Jazbinsek, K. Miyamoto, T. Omatsu, Y.S. Lee, O.P. Kwon, Terahertz Phonon Modes of Highly Efficient Electro-optic Phenyltriene OH1 Crystals, J. Phys. Chem. C 120 (2016) 24360–24369, doi:10.1021/acs.jpcc.6b07979.
[20] X. Zhang, X. Jiang, P. Liu, Y. Li, H. Tu, Z. Lin, D. Xu, G. Zhang, Y. Wu, J. Yao, Molecular design on isoxazolone-based derivatives with large second-order harmonic generation effect and terahertz wave generation, CrystEngComm 18 (2016) 3667–3673, doi:10.1039/C6CE00398B.
[21] S.J. Kwon, O.P. Kwon, J.I. Seo, M. Jazbinsek, L. Mutter, V. Gramlich, Y.S. Lee, H. Yun, P. Gunter, Highly Nonlinear Optical Configurationally Locked Triene Crystals Based on 3,5-Dimethyl-2-cyclohexen-1-one, J. Phys. Chem. 112 (2008) 7846–7852, doi:10.1021/jp711300w.
[22] T. Kolev, Z. Glavcheva, D. Yancheva, M. Schurmann, D.C. Kleb, H. Preut, P. Bleckmann, 2-{3-[2-(4-Hydroxyphenyl)vinyl]-5,5-dimethylcyclohex-2-en-1-ylidene}malononitrile, Acta Cryst. E 57 (2001) 0561–0562, doi:10.1107/S1600536801008480.
[23] Y. Li, Z. Wu, X. Zhang, L. Wang, J. Zhang, Y. Wu, Crystal growth and terahertz wave generation of organic NLO crystals: OH1, J. Cryst. Growth 402 (2014) 53–59, doi:10.1016/j.jcrysgro.2014.04.033.
[24] E.Y. Choi, M. Jazbinsek, J.H. Jeong, O.P. Kwon, Effect of ionic organic additives for the growth of polyene crystals synthesized by Knoevenagel condensations, CrystEngComm 14 (2012) 1045–1048, doi:10.1039/C1CE06018J.
[25] C. Hunziker, S.J. Kwon, H. Figi, F. Juvalta, O.P. Kwon, M. Jazbinsek, P. Günter, Configurationally locked, phenolic polyene organic crystal 2-{3-(4-hydroxystyryl)-5,5-dimethylcyclohex-2-enylidene}malononitrile: linear and nonlinear optical properties, J. Opt. Soc. Am. 25 (2008) 1678–1683, doi:10.1364/JOSAB.25.001678.
[26] S.J. Kwon, M. Jazbinsek, O.P. Kwon, P Gunter, Crystal growth and morphology control of OH1 organic electrooptic crystals, Cryst. Growth Des. 10 (2010) 1552–1558, doi:10.1021/cg900882h.
[27] H. Uchida, S.R. Tripathi, K. Suizu, T. Shibuya, T. Osumi, K. Kawase, Widely tunable broadband terahertz radiation generation using a configurationally locked polyene 2-[3-(4-hydroxystyryl)-5,5-dimethylcyclohex-2-enylidene] malononitrile crystal via difference frequency generation, Appl. Phys. B 111 (2013) 489–493, doi:10.1007/s00340-013-5362-0.
[28] MERCURY 1.3, Cambridge Crystallographic Data Centre, CCDC Software Limited, Cambridge, UK, 2004.
[29] J. Tauc, R. Grigorovici, A. Vancu, Optical Properties and Electronic Structure of Amorphous Germanium, Phys. Stat. Sol. (b) 15 (1966) 627–637, doi:10.1002/pssb.19660150224.
[30] M. Jazbinsek, U. Puc, A. Abina, A. Zidansek, Organic crystals for THz photonics, Appl. Sci. 9 (2019) 882, doi:10.3390/app9050882.
[31] S. Karthick, K. Thirupugalmani, G. Shanmugam, V. Kannan, S. Brahadeeswaran, Experimental and quantum chemical studies on N-H—O hydrogen bonded helical chain type Morpholinium 2-chloro-4-nitrobenzoate: A phasematchable organic nonlinear optical material, J. Mol. Struct. 1156 (2018) 264–272, doi:10.1016/j.molstruc.2017.11.115.
[32] Y. Takahashi, S. Onduka, S. Brahadeeswaran, M. Yoshimura, Y. Mori, T. Sasaki, Development of DAST crystals with high damage tolerance, Opt. Mater. 30 (2007) 116–118, doi:10.1016/j.optmat.2006.11.026.
[33] M. Rajkumar, M. Saravanabhavan, A. Chandramohan, Synthesis, structural, thermal, mechanical, second harmonic generation efficiency and laser damage threshold studies of 4-dimethylaminopyridinium-3,5-dicarboxybenzoate trihydrate single crystal, Opt. Mater. 72 (2017) 247–256, doi:10.1016/j.optmat.2017.06.011.
[34] T. Arumanayagam, P. Murugakoothan, Studies on growth, spectral and mechanical properties of new organic NLO crystal: Guanidinium 4-nitrobenzoate (GuNB), J. Cryst. Growth 362 (2013) 304–307, doi:10.1016/j.jcrysgro.2011.10.063.
[35] P. Srinivasan, T. Kanagasekaran, N. Vijayan, G. Bhagavannarayana, R. Gopalakrishnan, P. Ramasamy, Studies on the growth, optical, thermal and dielectric aspects of a proton transfer complex – Dimethyl amino pyridinium 4-nitrophenolate 4-nitrophenol (DMAPNP) crystals for non-linear optical applications, Opt. Mater. 30 (2007) 553–564, doi:10.1016/j.optmat.2007.01.014.
[36] P.M. Dinakaran, S. Kalainathan, Synthesis, growth, structural, spectral, linear and nonlinear optical and mechanical studies of a novel organic NLO single crystal 4-Bromo 4-Nitrostilbene (BONS) for nonlinear optical applications, Opt. Mater. 35 (2013) 898–903, doi:10.1016/j.optmat.2012.11.007.
[37] M. Krishnakumar, S. Karthick, G. Vinitha, K. Thirupugalmani, B. Babu, S. Brahadeeswaran, Growth, structural, linear, nonlinear optical and laser induced damage threshold studies of an organic compound: 2-Amino pyridinium-4-hydroxy benzoate, Mater. Lett. 235 (2019) 35–38, doi:10.1016/j.matlet.2018.09.148.
[38] K. Thirupugalmani, S. Karthick, G. Shanmugam, V. Kannan, B. Sridhar, K. Nehru, S. Brahadeeswaran, Second- and third-order nonlinear optical and quantum chemical studies on 2-amino-4-picolinium-nitrophenolate-nitrophenol: A phasematchable organic single crystal, Opt. Mater. 49 (2015) 158–170, doi:10.1016/j.optmat.2015.09.014.
[39] S. Karthick, D. Ganesh, K. Thirupugalmani, A.K. Chaudhary, S. Brahadeeswaran, Terahertz generation and optical properties of N-benzyl-2-methyl-4-nitroaniline single crystals in 0.1–2.0 THz range for photonic applications, Mater. Lett. 246 (2019) 95–98, doi:10.1016/j.matlet.2019.03.039.
[40] A. Markelz, A. Roitberg, E. Heilweil, Pulsed terahertz spectroscopy of DNA, bovine serum albumin and collagen between 0.1 and 2.0 THz, Chem, Phys. Lett. 320 (2000) 42–48, doi:10.1016/S0009-2614(00)00227-X.
[41] C.B. Reid, E.P. MacPherson, J.G. Laufer, A.P. Gibson, J.C. Hebden, V.P. Wallace, Accuracy and resolution of THz reflection spectroscopy for medical imaging, Phys. Med Biol. 55 (16) (2010) 4825–4838, doi:10.1088/0031-9155/55/16/013.
[42] R.I. Stantchev, D.B. Phillips, P. Hobson, S.M. Hornett, M.J. Padgett, E. Hendry, Compressed sensing with near-field THz radiation, Optica 4 (2017) 989–992, doi:10.1364/OPTICA.4.000989.
[43] F.L. Hirshfeld, Bonded-atom fragments for describing molecular charge densities, Theoret. Claim. Acta (Berl.) 44 (1977) 129–138, doi:10.1007/bf00549096.
[44] M.A. Spackman, P.G. Byrom, A novel definition of a molecule in a crystal, Chem. Phys. Lett. 267 (1997) 215–220, doi:10.1016/S0009-2614(97)00100-0.
[45] M.A. Spackman, D. Jayatilak, Hirshfeld surface analysis, CrystEngComm 11 (2009) 19–32, doi:10.1039/B818330A.
[46] S.K. Wolff, D.J. Grimwood, J.J. McKinnon, M.J. Turner, D. Jayatilaka, M.A. Spackman, Crystal Explorer 3.1, University of Western Australia, Crawley, Australia, 2012.
[47] K. Raju, M. Aruchamy, S. Karuppannan, Single Crystal Growth of N-Benzyl-2-methyl-4-nitroaniline by Seeded Czochralski Pulling Technique for NLO and THz Applications, Cryst, Res. Technol., 55, 2020 1900234, doi:10.1002/crat.201900234.